

Koutsou, A., Christodoulou, C. , Bugmann, G. and Kanev, J. (2012). Distinguishing the Causes of Firing with the Membrane Potential Slope. *Neural Computation*, doi: 10.1162/NECO\_a\_00323  
(accepted March 1, 2012, in press)

1

## **Distinguishing the Causes of Firing with the Membrane Potential Slope**

**Achilleas Koutsou**

*achilleas.k@cs.ucy.ac.cy*

**Chris Christodoulou**

*cchrist@cs.ucy.ac.cy*

*Department of Computer Science, University of Cyprus,  
75 Kallipoleos Avenue, P.O. Box 20537, 1678 Nicosia, Cyprus*

**Guido Bugmann**

*gbugmann@plymouth.ac.uk*

*Centre for Robotic and Neural Systems, University of Plymouth,  
Drake Circus, PL4 8AA, Plymouth, United Kingdom*

**Jacob Kanev**

*j\_kanev@arcor.de*

*Dept. of Electrical Engineering and Computer Science, Technische Universität Berlin,  
10587 Berlin, Germany*

**Keywords:** membrane potential slope, coincidence detection, temporal integration.

### **Abstract**

In this letter, we aim to measure the relative contribution of coincidence detection and temporal integration to the firing of spikes of a simple neuron model. To this end, we develop a method to infer the degree of synchrony in an ensemble of neurons whose firing drives a single, post-synaptic cell. This is accomplished by studying the effects of synchronous inputs on the membrane potential slope of the neuron and estimating the degree of response-relevant input synchrony, which determines the neuron's operational mode. The measure is calculated using the normalised slope of the membrane potential

prior to the spikes fired by a neuron and we demonstrate that it is able to distinguish between the two operational modes. By applying this measure to the membrane potential time course of a leaky integrate-and-fire neuron with the partial somatic reset mechanism, which has been shown to be the most likely candidate to reflect the mechanism used in the brain for reproducing the highly irregular firing at high rates, we show that the partial reset model operates as a temporal integrator of incoming excitatory post-synaptic potentials and that coincidence detection is not necessary for producing such high irregular firing.

## 1 Introduction

The firing patterns of neurons are traditionally considered to be random (Perkel, Gerstein & Moore, 1967a,b; Stein, 1967; Softky & Koch, 1992, 1993; Shadlen & Newsome, 1994, 1995, 1998; Stein, Gossen & Jones, 2005; Kostal, Lánský & Rospars, 2007), an assumption which suggests that the relative timing of individual spikes is of no consequence. However, there are studies which show that the activity of neurons is often correlated and synchronised (Usrey & Reid, 1999; Salinas & Sejnowski, 2001; Buzsáki & Draguhn, 2004) and there has been a growing number of recent publications focusing on ways to detect and measure correlations and synchronous events in neural spiking (Faes et al., 2008; Schrader et al., 2008; Stark & Abeles, 2009; Staude, Rotter & Grün, 2010; Grün, Diesmann & Aertsen, 2010; Kreuz et al., 2011). The role and significance of correlated activity and synchrony has been a matter of theoretical study for the last few decades (von der Malsburg, 1981; Abeles, 1982; Crick & Koch, 1990; König, Engel & Singer, 1996; Singer, 1999).

An important aspect of synchronous activity in a neural ensemble, one that is often overlooked, is the effect it can have on the behaviour of a single, common post-synaptic neuron. The degree of pre-synaptic synchrony has been linked to the continuum between the two operational modes considered to be employed by cortical neurons, namely temporal integration and coincidence detection (König, Engel & Singer, 1996; Aertsen, Diesmann & Gewaltig, 1996; Kisley & Gerstein, 1999; Rudolph & Destexhe, 2003). More specifically, Aertsen, Diesmann & Gewaltig (1996) showed that higher synchronisation at the input leads to shorter response latency and a higher probability

of response (i.e., response reliability), which are two of the main characteristics of coincidence detection. This was later reinforced by Rudolph & Destexhe (2003), who used a conductance-based compartmental neuron model and showed that the neuron is able to operate as both a temporal integrator or a coincidence detector, depending on the degree of input synchrony. These authors also emphasised that the two operational modes lie at the two extremes of a continuum with no discrete boundary between the two modes (Rudolph & Destexhe, 2003). Additionally, coincidence detection has been proposed as a candidate mechanism for the highly irregular, high rate firing observed in cortical cells; in particular, Softky & Koch (1992, 1993), in an attempt to reproduce such experimental recordings from cortical cells in the primary visual (V1) and middle temporal visual (MT) areas, concluded that temporal integration was an unlikely mechanism for cortical neurons exhibiting this behaviour, as integrators have very regular firing patterns at such high rates. They suggested that coincidence detection is a more likely operational mode. Bugmann, Christodoulou & Taylor (1997) and Christodoulou & Bugmann (2001) demonstrated that incomplete post-spike re-polarisation of the membrane was the most likely candidate for producing highly irregular firing at high rates, with independent exponentially distributed intervals. However, they were unable to provide a conclusive answer as to whether the model operates predominantly as a coincidence detector or temporal integrator, when exhibiting highly irregular, high rate firing behaviour.

Discovering if cortical neurons are driven by synchronous volleys of spikes and if so, measuring the degree of synchrony, would provide an important step towards a solution to the problem of understanding the neural code. If the firing of the pre-synaptic ensemble of a neuron is highly synchronised, the post-synaptic neuron operates as a coincidence detector. This implies a high temporal precision for the neural code, which in turn implies that a temporal code is most likely being employed, rather than a rate code. Therefore, a potential method of measuring the degree of firing-relevant synchrony at the input of a neuron would be a valuable tool for solving the problem of the neural code.

While multi-neuron recordings are becoming increasingly easier and more common to perform (Schrader et al., 2008; Staude, Rotter & Grün, 2010; Berger et al., 2010), identifying the thousands of neurons that act as inputs to a single cell and recording their

activity is not a trivial task. It is therefore preferable and simpler to develop a method of inferring the degree of synchrony between the inputs of a neuron by observing the fluctuations of the neuron's membrane potential. Kisley & Gerstein (1999) for example, demonstrated that the slope of the membrane potential directly preceding a spike is indicative of the level of synchrony in a neuron's pre-synaptic ensemble. Additionally, DeWeese & Zador (2006) studied intracellular recordings of cells in the auditory cortex of the rat and discovered that rapid fluctuations in the membrane potential most likely indicate brief, synchronous volleys of spikes. Very recently, Kobayashi, Shinomoto & Lánský (2011) studied the membrane potential fluctuations of a simple neuron model in order to infer the pre-synaptic input rates. Goedeke & Diesmann (2008) showed that the response of a simple neuron model to synchronised inputs is dependent on the membrane potential and its derivative. They emphasised that in addition to the membrane potential, the derivative should also be considered when studying neural synchronisation in feed-forward networks (Goedeke & Diesmann, 2008).

These studies show that the firing properties of the pre-synaptic ensemble, especially properties relating to synchrony, are reflected in the time course of the intracellular membrane potential of the post-synaptic neuron. It should therefore be possible to establish an invertible relationship between the input and the membrane potential in order to infer the pre-synaptic firing properties from the membrane potential data.

Pre-synaptic synchrony has been known to also affect the post-synaptic neuron's firing patterns. In particular, it has been shown that correlated inputs affect the firing rate (Kuhn, Rotter & Aertsen, 2002) as well as the firing irregularity (Salinas & Sejnowski, 2002) of the post-synaptic neuron. While these effects can be seen in the firing inter-spike interval (ISI) distribution, the same properties (rate and irregularity) are also affected by the rest of the input features. Furthermore, the effects of higher correlations on the firing statistics differ depending on other properties of the neuron or its inputs. It is unlikely that any inferences can be made regarding the input synchrony from observations of the neuron's firing statistics alone. The trajectory of the membrane potential of the post-synaptic neuron provides much more information regarding the activity of the pre-synaptic population.

In order to determine where the operational mode of a given neuron lies on the continuum between temporal integration and coincidence detection, we studied the cor-

relation between the slope of the membrane potential, within a short period of time prior to firing, with the degree of pre-synaptic synchrony. In this regard, it is analogous to the spike-triggered average stimulus (also known as the reverse correlation between the spike train and stimulus; Mainen & Sejnowski, 1995; Bugmann, Christodoulou & Taylor, 1997). As such, analytical treatments of the spike-triggered average could be adapted to study and calculate the expected shape of the pre-spike membrane potential, in place of the stimulus (Kanev, Wenning & Obermayer, 2004).

In the rest of this letter, we initially describe the models used, their parameters and how our measure is calculated. We then describe how our simulations were set up and run, in order to establish the reliability of our measure and subsequently, to measure the operational mode of a neuron firing highly irregular spike trains at high rates. We continue with presenting our results and conclude with a detailed discussion including comparison of our study and results with related work.

## 2 Methodology

### 2.1 Models

In this study we used the leaky integrate-and-fire (LIF) neuron model, also known as the Lapique model (Lapique, 1907; Tuckwell, 1988), as well as a variant of the LIF model which uses a partial reset mechanism (LIFwPR) (Bugmann, Christodoulou & Taylor, 1997).

#### Leaky Integrate-and-Fire (LIF) neuron model

The LIF model describes the time course of the membrane potential for sub-threshold voltages:

$$\frac{dV}{dt} = \frac{-(V(t) - V_{rest}) + RI(t)}{\tau_m} \quad (1)$$

where  $V(t)$  is the membrane potential at time  $t$ ,  $V_{rest}$  is the resting potential, i.e., the membrane potential at the initial time  $t_0$  such that  $V(t_0) = V_{rest}$ . Furthermore,  $R$  is the resistance of the membrane and  $\tau_m$  is the membrane leak time constant.  $I(t)$  is the time-dependent input, which is modelled as a time varying function or as a random spike generator process (e.g., a Poisson generator; Stein, 1965).

The firing mechanism of the model is triggered explicitly when the membrane potential reaches a fixed threshold  $V_{th}$ , after which the membrane potential is reset back to  $V_{rest}$ . A refractory period is modelled by disabling the firing mechanism for a short period,  $t_r$ , after a spike is fired. The values of the model parameters used for the simulations in this paper are listed in Table 1.

### **Partial reset LIF variant (LIFwPR) neuron model**

The LIFwPR variant of the LIF model sets the membrane potential following the firing of a spike, at a level higher than the resting potential, i.e.,  $V_{reset} > V_{rest}$  (Lánský & Smith, 1989; Lánský & Musila, 1991; Bugmann, Christodoulou & Taylor, 1997). This models the incomplete electrical decoupling between the neuron's soma and dendrites (Rospars & Lánský, 1993; Lánský & Rodriguez, 1999). In Bugmann, Christodoulou & Taylor (1997), it was shown that the LIFwPR is equivalent to a LIF with a time-dependent threshold (Wilbur & Rinzel, 1983; Tuckwell, 1988). The level of reset is controlled by the reset parameter  $\beta$ , which relates  $V_{reset}$  to the threshold and resting potential:

$$V_{reset} = \beta (V_{th} - V_{rest}) + V_{rest} \quad (2)$$

The LIFwPR model was chosen for its ability to produce highly variable firing at high rates, consistent with experimental recordings (Softky & Koch, 1993), particularly when  $\beta = 0.91$ , as proved by Bugmann, Christodoulou & Taylor (1997), which results in a reset potential of  $V_{reset} = 13.65$  mV. Setting  $\beta = 0$ , the model becomes a LIF ( $V_{reset} = V_{rest}$ ).

### **Description of the inputs**

Synaptic inputs were modelled in all cases as realisations of a Poisson process (i.e., intervals were exponentially distributed). The input population was characterised by five parameters, two of which relate to synchrony. The non-synchrony parameters are the number of input spike trains ( $N_{in}$ ), the average rate of the inputs ( $f_{in}$ ) and the level of depolarisation caused by each spike on the membrane potential ( $\Delta V_s$ ). In addition, the two parameters which defined the level of synchrony are (i)  $S_{in}$ , which denotes the proportion of spike trains which are synchronous and (ii)  $\sigma_{in}$ , which is the standard

deviation of a normally distributed random variable that is used to apply Gaussian jitter to each individual spike in the identical spike trains. The parameter ranges were chosen such that our measure is investigated in the entire dynamic range of the LIF model. More specifically, spike trains are generated by performing the following steps:

1. Generate one Poisson spike train, with rate  $f_{in}$  for the length of the simulation  $T$ .
2. Copy the generated spike train  $(S_{in}N_{in} - 1)$  times, giving a total of  $S_{in}N_{in}$  identical spike trains.
3. For each spike in all spike trains generated so far, shift its time by a random variate drawn from a normal distribution  $X \sim \mathcal{N}(0, \sigma_{in}^2)$ .
4. Generate  $(1 - S_{in})N_{in}$  Poisson spike trains, giving a total of  $N_{in}$  input spike trains.

The product  $S_{in}N_{in}$  is always rounded to the nearest integer. Fig. 1 shows three sample input cases. The raster plots show the effect of the two variables  $S_{in}$  and  $\sigma_{in}$  on the overall synchrony of the spike trains. Each input spike causes an instantaneous jump of  $\Delta V_s$  in the post-synaptic neuron's membrane potential.

The maximum value for  $\sigma_{in}$  of 4 ms (see Table 1 for ranges and values for all parameters) was chosen such that it is high enough to reduce synchrony significantly, to the point where no synchronous activity beyond what is expected by random chance remains, even for cases where  $S_{in} = 1$ .

Note that, while various input parameter ranges were investigated for the LIF model, the parameters of the LIFwPR model are constant (Table 1). These values were taken from Bugmann, Christodoulou & Taylor (1997) who investigated the LIFwPR model and determined the parameter values which cause highly irregular high rate firing. Therefore, an investigation of the parameters of the LIFwPR model is outside the scope of our work, as we employ the specific model solely to investigate its sub-threshold membrane potential trajectories in the highly irregular high firing rate regime.

Our study focused exclusively on excitatory inputs. This simplifying assumption allowed us to define more clearly the effects of synchronous activity on the membrane potential trajectory in a more predictable fashion. Even though we previously demonstrated (Christodoulou et al., , 2000) that increasing inhibition leads to greater membrane potential fluctuations apart from reducing the mean membrane potential, the

effects of inhibition on the slope of the membrane potential, in the presence of synchronous activity, is a subject of ongoing work.

Parameter	LIF value or range	LIFwPR value or range
$V_{th}$	15 mV	15 mV
$V_{rest}$	0 mV	0 mV
$V_{reset}$	0 mV	13.65 mV
$R$	10 k $\Omega$	10 k $\Omega$
$\tau_m$	10 ms	10 ms
$t_r$	2 ms	2 ms
$\Delta V_s$	0.1 mV – 2.0 mV	0.16 mV
$N_{in}$	30 – 200	50
$f_{in}$	20 Hz – 700 Hz	150 Hz – 300 Hz
$S_{in}$	0 – 1	0 – 1
$\sigma_{in}$	0 ms – 4 ms	0 ms – 4 ms

Table 1: Parameter values for the models used in this study. Many of the parameters share a common value; we list them explicitly for completeness. The ranges of the input rates were chosen accordingly to study the entire obtainable firing frequency range.

## 2.2 Methods

The two models, the LIF and LIFwPR variant, were used to study the relationship between the slope of the membrane potential prior to the firing of a spike and the amount of synchrony which exists in the input spike trains that caused the firing. Determining a relationship between the two will allow us to develop a method that can reliably measure the response-relevant input synchrony and by extension, the neuron’s operational mode.

### Pre-spike membrane potential slope

Since the time course of the membrane potential is discontinuous due to input spikes causing instantaneous jumps in the membrane potential, we define a temporal window of length  $w$ , which we call the *coincidence window*. This allows us to calculate the membrane potential's average rate of change between  $t_i$  and  $t_i - w$ , where  $t_i$  is the moment when the  $i^{th}$  spike was fired. In other words, we calculate the slope of the secant line that intersects the membrane potential trace at the start and end of the window  $w$  (fig. 2a), as shown in eqn. (3),

$$m_i = \frac{V(t_i) - V(t_i - w)}{w}, \quad (3)$$

where  $V(t)$  denotes the membrane potential at time  $t$ . Note that  $V(t_i)$  is the membrane potential during the firing of a spike and therefore  $V(t_i) = V_{th}$ .

### Normalisation bounds

In order to associate the pre-spike slope of the membrane potential with the level of pre-synaptic synchrony and the operational mode continuum, we define the values of the slope  $m_i$  for the two limiting cases, i.e., completely synchronous ( $S_{in} = 1$ ) and completely random ( $S_{in} = 0$ ) inputs. No jitter is assumed in either case ( $\sigma_{in} = 0$  ms). Each limiting case corresponds to a bound in the operational mode continuum.

For  $S_{in} = 0$ , inputs are completely random and coincidences between spikes occur due to random chance alone. The post-synaptic neuron integrates the random inputs and fires spikes in response to an almost constant arrival of spikes, with very small fluctuations. The membrane potential of the neuron in this case, rises almost steadily from  $V_{rest}$  to  $V_{th}$  during each inter-spike interval (ISI). The value of the lower normalisation bound is therefore defined as:

$$L_i = \frac{V_{th} - \left( V_{rest} + I \left( 1 - \exp \left( -\frac{\Delta t_i - w}{\tau_m} \right) \right) \right)}{w} \quad (4)$$

where  $\Delta t_i$  is the length of the ISI preceding the  $i^{th}$  spike and  $I$  is the constant input required to fire at the end of the ISI, starting from  $V_{rest}$ :

$$I = \frac{V_{th} - V_{reset}}{1 - \exp \left( -\frac{\Delta t_i}{\tau_m} \right)} \quad (5)$$

The lower bound therefore varies for each spike in a spike train.

Eqn. (4) assumes a membrane potential generated by a classical LIF. In the case of the LIFwPR however, a constant arrival of spikes would cause the pre-spike membrane potential slope to be lower, since the potential of the membrane at the start of each ISI is not  $V_{rest}$  but  $V_{reset}$  (fig. 2b). We therefore redefine the lower bound to account for the LIFwPR as:

$$L_i^* = \frac{V_{th} - \left( V_{reset} + I \left( 1 - \exp \left( -\frac{\Delta t_i - w}{\tau_m} \right) \right) \right)}{w} \quad (6)$$

For  $S_{in} = 1$ , the neuron receives  $N_{in}$  spikes simultaneously at random (exponentially distributed) intervals. If  $N_{in}\Delta V_s \geq (V_{th} - V_{rest})$ , each volley of spikes causes the neuron to fire. Assuming a classical LIF model, the membrane potential prior to firing remains at  $V_{rest}$  up to the moment of firing  $t_i$ , when it instantaneously jumps to  $V_{th}$ . Since we cannot define the slope of the instantaneous jump, we use the same temporal window  $w$  as described for eqn. (3) and the value of the upper normalisation bound is defined as:

$$U_i = \frac{V_{th} - V_{rest}}{w}. \quad (7)$$

In the case of the LIFwPR, eqn. (7) must also account for the higher potential of the membrane at the start of the ISI. More specifically, to determine the upper normalisation bound, we must calculate the membrane potential at the start of the coincidence window, after it has decayed from  $V_{reset}$  (fig. 2b). The underlying assumption is that in the case of complete synchrony ( $S_{in} = 1$ ), no inputs arrive between volleys and the potential is affected only by the leak term. The redefined upper normalisation bound is therefore:

$$U_i^* = \frac{V_{th} - \left( V_{rest} + (V_{reset} - V_{rest}) \exp \left( -\frac{\Delta t_i - w}{\tau_m} \right) \right)}{w}. \quad (8)$$

The term  $\left( V_{rest} + (V_{reset} - V_{rest}) \exp \left( -\frac{\Delta t_i - w}{\tau_m} \right) \right)$  defines the membrane potential after it has decayed from  $V_{reset}$  for a period  $(\Delta t_i - w)$ . In other words, it is the membrane potential at the start of the coincidence window, for the limiting case of complete synchrony.

When analysing data generated from a LIF neuron, the two variations on the lower and upper bounds (eqns. (6) & (8)) behave identically to the standard forms (eqns. (4) & (7)), due to the fact that for the LIF  $V_{rest} = V_{reset}$ .

The bounds are used to linearly normalise the pre-spike membrane potential slope  $m_i$  for each spike to fall within the range [0-1]:

$$M_i = \frac{m_i - L_i}{U_i - L_i}. \quad (9)$$

For the LIFwPR model, the bounds  $U_i^*$  and  $L_i^*$  are used accordingly.

### The role of the coincidence window

The coincidence window  $w$  defines a period in which all input spikes within it are regarded as coincident (synchronous). Coincidence to arbitrary precision is unlikely, although much more probable when binning data due to a simulation time step. The length of  $w$  defines the precision of coincidences explicitly.

The role of  $w$  becomes clear when one considers how it affects the calculation of the slope in the limiting case of high synchrony. For a LIF neuron, if the membrane potential at the start of the window is at the resting potential, i.e.,  $V(t_i - w) = V_{rest}$ , then this means that enough spikes arrived within a period  $w$  to cause the neuron to fire from rest. The slope, as calculated by eqn. (3) will not be affected, irrespective of whether these input spikes were completely synchronised or not. In other words, all spikes responsible for the firing that arrived between  $(t_i - w)$  and  $t_i$  and the resulting slope will become equal to the upper normalisation bound  $U_i$ .

More generally, we may consider an arbitrary initial potential,  $V(t_i - w) = u$ . The temporal dispersion of the spikes arriving within the coincidence window has no effect on eqn. (3), the result of which would always be  $\frac{V_{th} - u}{w}$ . The value of  $w$  is therefore a measure of the assumed temporal precision of the neural code and its length allows one to change the temporal resolution of the slope calculation, to match the theoretical limits of a neural temporal code.

For our simulations, we set the parameter  $w = 2$  ms, since it has been noted that for neurons with membrane time constants within the range of 10–20 ms, a temporal code with accuracy between 1–3 ms is theoretically possible (Gerstner et al., 1996). By setting the width of the coincidence window to 2 ms, we effectively attempt to measure the level of synchrony of the input spikes that caused each response, under the assumption that the temporal precision of coincidence detection is 2 ms.

## 2.3 Simulation details

Simulations of the models described in section 2.1 were implemented using the Runge-Kutta (RK4) approximation of the derivative with a simulation time-step of 0.1 ms (Wilson, 1999). Other methods could have been used for iteratively solving the differential equations which describe the models, such as the ‘Exact Integration’ method by Rotter & Diesmann (1999). Each simulation ran for  $T = 10$  s of simulated time.

Simulations were run in configuration sets where  $\Delta V_s$  and  $N_{in}$  were kept constant for all simulations in the set. Additionally, a target firing rate  $f_{out}$  was defined for the configuration set. Each simulation in a set was assigned a unique combination of  $S_{in}$  and  $\sigma_{in}$  values. For each synchrony parameter pair, the input rate  $f_{in}$  was calibrated accordingly to obtain the desired target firing rate  $f_{out}$ . The appropriate input rate was determined by iteratively increasing or decreasing  $f_{in}$  until the desired  $f_{out}$  was obtained. This calibration was necessary because the synchrony parameters affect the neuron’s firing rate and since our measure relies on the firing ISIs, simulations which share the same firing rate are more comparable. Additionally, one of the objectives of the current work is to study the highly irregular, high firing rate regime, using the LIFwPR neuron. It is therefore more appropriate to group simulations and results based on the neuron’s firing rate, to allow us to separate simulations and results which belong to a low or high firing rate regime.

The simulations of the LIF neuron aimed at establishing the relationship between the synchrony parameters and the mean value of  $M_i$  for the entire simulation. The LIFwPR simulations on the other hand were subsequently used to determine the operational mode of the model when firing highly irregular spike trains at high rates.

## 3 Results

### 3.1 Results with the LIF neuron model

The six contour plots in fig. 3 show results of simulations of the LIF neuron for various parameter combinations (see figure caption for details). The parameters were chosen to demonstrate how the measure behaves under various input regimes (described in section 4). The plots show the mean normalised pre-spike slope of the membrane potential ( $\overline{M}$ )

for all combinations of  $S_{in}$  and  $\sigma_{in}$  within the value ranges specified in Table 1. Each  $\overline{M}$  value represents the mean  $M$  for all spikes fired during  $T = 10$  s of simulated time.

The value of  $\overline{M}$  reaches the maximal value of 1 in the lower right hand corner, which corresponds to completely synchronised input spike trains ( $S_{in} = 1$ ) with no jitter ( $\sigma_{in} = 0$  ms). As expected, increasing the amount of jitter (higher  $\sigma_{in}$  values, i.e., moving up on the contour plot), decreases the value of  $\overline{M}$ . The correlation coefficient between  $\sigma_{in}$  and  $\overline{M}$ , when  $S_{in} = 1$ , is  $\rho_{\sigma, M} = -0.95$  indicating a very high, negative linear relationship. Similarly, less synchronised spike trains (lower  $S_{in}$  values, i.e., moving left on the plot) also decrease the value of  $\overline{M}$ . The correlation between  $S_{in}$  and  $\overline{M}$ , when  $\sigma_{in} = 0$  ms, shows a near perfect positive linear relationship, with a correlation coefficient of  $\rho_{S, M} = 0.99$  (clearly shown in fig. 4). These values correspond to a desired  $f_{out} = 70$  Hz (corresponding to fig. 3d).

The results shown in fig. (3) and the strong correlation between the input parameters and  $\overline{M}$  (fig. 4) discussed above indicate that our method can reliably detect and measure input synchrony which was relevant to the firing of response spikes. The method maintained a high reliability for a wide range of the input parameter values, i.e., the number of spike trains ( $N_{in}$ ), the desired firing rate ( $f_{out}$ ) and the membrane potential rise per spike ( $\Delta V_s$ ). However, the robustness of this correlation depends on the input regime, i.e., the strength of the input volleys with respect to the firing threshold. In particular, this correlation between input synchrony and measured  $\overline{M}$  is robust as long as the synchronous volleys are super-threshold (see section 4 for details).

Of particular interest is the case where the LIF neuron is driven by high rate inputs causing it to fire at extremely high rates. Fig. 3f shows the measured synchrony of a LIF neuron with  $f_{out} = 400$  Hz. Comparing this plot to the others of fig. 3, it is evident that the value of  $\overline{M}$  is higher than expected when there are very low degrees of input synchrony. This can be seen in the lower part of the synchrony parameter range, i.e., the upper left half of the plot, which has a darker shade than in the cases with lower firing rates (fig. 3a – 3e). Additionally, the value of  $\overline{M}$  is lower than expected at higher ranges of the synchrony spectrum, as can be seen by the darker areas in fig. 3f being considerably smaller than the dark, high synchrony areas of the other plots.

These unexpected results (fig. 3f) are due to the mean firing ISI approaching in length to the coincidence window. More specifically, if an ISI is equal to the coincidence

window  $\Delta t_i = w$ , then the values of the two bounds (eqns. (6) & (8)) become equal. This occurs because in such circumstances, the firing of a spike due to integration of inputs within a period equal to the ISI is equivalent to firing solely from input spikes arriving within a period  $w$ . We can investigate the divergent behaviour between the two modes as a function of the ISI ( $\Delta t_i$ ) and coincidence window length ( $w$ ). To accomplish this, we define the level of divergence (or *relative difference*) between the perfect, non-leaky Integrate-and-Fire model (PIF), which represents perfect integration and the LIF model. The relative difference indicates the degree by which the PIF model differs from the LIF. It is calculated as the difference between the values of the membrane potential of the two models (LIF and PIF), divided by the membrane potential of the original model, i.e., the LIF, at the start of the coincidence window, in order to estimate how well the PIF model approximates the pre-spike slope values of the LIF (see Appendix A for details). The lower the relative difference, which occurs at higher firing rates, the more similar the two modes become. This leads to less accurate results as the distance between the two models and by extension, the two bounds becomes smaller. Fig. 5 shows the relative difference ( $d$ ) as a function of the firing ISI, for a fixed window length  $w = 2 \text{ ms}$  (see eqn. (13) in Appendix A). This analysis supports that the two operational modes, as defined in this work, display a convergent behaviour as firing rates increase (i.e., the relative difference  $d$ , also known as the level of divergence, becomes smaller). The very low relative difference between the two models at firing rates of 400 Hz ( $d_{2.5 \text{ ms}} = 0.025$ ) is the reason why the metric produces unexpected results for analysing data for this particular extremely high rate firing. In such a case, the two modes of operation are too similar to be reliably distinguished.

### 3.2 Results with the LIF neuron model with partial reset (LIFwPR)

We also measured the normalised pre-spike membrane potential slope of a model neuron exhibiting highly irregular firing at high rates. We used the LIFwPR, with neuron and input parameter values identical to the model by Bugmann, Christodoulou & Taylor (1997). The inputs to the neuron consisted of 50 Poisson spike trains and each input spike caused a depolarisation of the neuron's membrane potential by  $\Delta V_s = 0.16 \text{ mV}$ . We used a reset parameter value of  $\beta = 0.91$  as it has been shown to be the only value

that can produce purely temporally irregular firing (with no bursting activity that can increase the firing variability) (Bugmann, Christodoulou & Taylor, 1997; Christodoulou & Bugmann, 2001). This is compatible with the high firing irregularity at high rates observed in cortical neurons (Softky & Koch, 1992, 1993).

The results (fig. 6) show the value of  $\overline{M}$  being always below 0.1, for the entire range of firing rates. Each firing rate was achieved by varying input rates within physiological ranges. These results suggest that neurons firing highly irregularly at high rates operate mainly as temporal integrators.

In Bugmann, Christodoulou & Taylor (1997), it was suggested that temporal integration and fluctuation detection (i.e., coincidence detection) can coexist and cause irregular firing, which was indicated by the ISI of a LIFwPR neuron driven by a fluctuating input current being significantly shorter than the ISI of the same neuron driven by a constant input current (of the same average value). The current results however indicate that there is a strong dominance of temporal integration and the relatively small contribution of coincidence detection in the firing of spikes is not sufficiently high to be distinguishable from the effects of the temporal integration process. This indicates that coincidence detection is not necessary for producing highly irregular firing at high rates (which was suggested by Softky & Koch, 1992, 1993) and that temporal integration on its own is sufficient for such a purpose, provided the neuron does not completely repolarise.

It has to be pointed out however, that our results are not incompatible with the analysis by Softky & Koch (1993). In their analysis, these authors express the threshold in number of input pulses,  $N_{th}$ , necessary to raise the neuron's membrane potential from rest to discharge. With the partial reset mechanism, the LIFwPR neuron's membrane potential stays very close to the spike threshold during most of the time in a trial's duration, assuming the neuron is spiking at high enough rates. More importantly, the membrane potential is almost always above the reset potential  $V_{reset}$  after the first spike is fired. With this in mind, we have shown (see Appendix B) that when the LIFwPR neuron is driven by sufficiently frequent arriving inputs, it operates equivalently to a neuron with an effective resting potential  $V'_{rest}$  equal to the reset potential  $V_{reset}$ ; this results in (i) a reduction of the effective number of inputs required to fire a spike and (ii) a very short (sub-millisecond) effective membrane leak time constant. As it can be

seen from Appendix B, for our simulations  $N'_{th}$  is approximately 9 and  $\tau'_m$  is a function of the membrane potential  $V(t)$  and takes values less than 1 ms ( $\leq 0.9$  ms).

Our results are thus in accord with the analysis by Softky & Koch (1993) who showed that for low  $N_{th}$  values and sub-millisecond membrane time constant  $\tau_m$ , a LIF neuron operating as a temporal integrator can fire highly irregularly at high rates (see fig. 8 in Softky & Koch, 1993). From the above analysis, we can therefore conclude that the LIFwPR model, which models the incomplete post-spike re-polarisation of a neuron, can be used for (i) reducing the effective number of input spikes  $N'_{th}$  required to cause a spike and (ii) decreasing the effective membrane leak time constant  $\tau'_m$  such that a neuron can fire highly irregularly at high rates, in accordance with experimental recordings. Moreover, it has to be noted that the LIFwPR model, apart from modelling more accurately different firing regimes, it has also been shown (i) to be able to reproduce experimental firing statistics (as shown by Bugmann, Christodoulou & Taylor, 1997, on the data analysed by Softky & Koch, 1992, 1993) and (ii) that it enhances learning (Christodoulou & Cleanthous, 2011; Cleanthous & Christodoulou, 2012).

## 4 Discussion

Our study establishes the correlation between input synchrony  $S_{in}$  and the slope of the membrane potential prior to firing  $m$ . This depends on normalising the slope between two bounds. Our results suggest a strong correlation between pre-spike membrane potential slope and pre-synaptic synchrony levels, that allow us to infer the degree of response-relevant input synchrony under certain assumptions, namely the existence of excitation only and of super-threshold volleys. The measure is robust against the value of the average stimulus, i.e., whether it is super- or sub-threshold. In the very rare case where firing results from the integration of a burst of multiple coincident sub-threshold volleys, the measure will underestimate the synchrony. In a theoretical study, Stein (1967) showed that the slope of the membrane potential is inversely proportional to the variance of the firing ISIs, for a neuron driven by Poisson inputs. Goedeke & Diesmann (2008) showed that the membrane potential, as well as its derivative, define the response of a LIF model to synchronised inputs. They analytically studied the dynamics of the behaviour of a LIF neuron, both in isolation and in homogeneous networks and

concluded that the synchronisation between neurons depends both on the membrane potential and its derivative. While these studies prove the existence of a correlation between membrane potential and firing statistics of both individual neurons and networks, our own work establishes a specific correlation measure between membrane potential and input statistics. As such, the two results may be considered complimentary.

However, a potential correlation between firing and input statistics is most likely not as straightforward to investigate, since both the membrane potential fluctuations and the firing ISI distribution are affected by multiple parameters of the stimulus. As already mentioned, synchrony in the pre-synaptic activity of a neuron can affect its firing rate (Kuhn, Rotter & Aertsen, 2002) and irregularity (Salinas & Sejnowski, 2002). However, these effects are not consistent and depend heavily on the state of the neuron. More precisely, the output firing rate is a non-monotonic function of the correlation among excitatory inputs (Kuhn, Rotter & Aertsen, 2002). Additionally, the firing variability depends heavily on other factors besides the degree of input correlations (Salinas & Sejnowski, 2002). Our measure relies on the assumption that changes in input parameters are reflected in the trajectory of the membrane potential, while similar changes may not affect the distribution of firing ISIs in a consistent manner.

Our work is more closely related to Kisley & Gerstein (1999) and more recently to DeWeese & Zador (2006) and Kobayashi, Shinomoto & Lánský (2011), in that we establish a relationship between membrane potential properties and properties of the input spike trains, in order to infer the latter from measurements of the former. DeWeese & Zador (2006) analysed membrane potential dynamics to infer properties of the input population. Similarly, Kobayashi, Shinomoto & Lánský (2011) developed an algorithm to estimate the time-varying input rates of the pre-synaptic population by studying the membrane potential of the neuron. The correlation between membrane potential slope and input synchrony was studied by Kisley & Gerstein (1999). The work presented in this article relies on this correlation to provide a measure of the response-relevant input synchrony, which relates to the operational mode of the neuron. In particular, the normalised pre-spike membrane potential slope provides a measure of the relative contribution of temporal integration and coincidence detection to the firing of a spike, or the operation of a neuron in general.

The choice of the length of the coincidence window, i.e., the value of  $w$ , is an

important aspect of our metric calculation. It has to be noted that the effect of this variable on the temporal precision of firing has also been the subject of a rigorous theoretical study (Reed, Blum & Mitchell, 2002; Mitchell, 2005). As mentioned in section 2.2, the value of this parameter should reflect the time that is regarded as the maximum temporal distance between two events that are considered to be coincident (2 ms in our case). The only limit for the length of the coincidence window is the time step of the simulation (here 0.1 ms) or more generally, the temporal resolution of the data being analysed. However, the smaller the value of  $w$ , the stricter the definition of coincident activity becomes, which in turn produces lower  $\overline{M}$  values, unless the input spike trains are completely synchronised. This provides a degree of flexibility for the metric calculation that allows it to be adapted to various levels of temporal resolution.

The meaning of the value for the length of the coincidence window can be intuitively understood in terms of the cost parameter found in spike train distance metrics (see Victor & Purpura, 1996; Victor, 2005; Kreuz et al., 2011), which controls the sensitivity of the metric to spike count and spike timing, i.e., the assumed resolution of the temporal code. Spike train distance metrics measure the distance between two spike trains by calculating the minimum cost of transforming one spike train into the other by adding, removing or shifting spikes. By manipulating the cost parameter, one can control the measured distance between two given spike trains. For instance, with a small cost parameter value, two very different spike trains will be measured as having a small distance, i.e., they are considered similar by the metric due to the low cost of shifting spikes. Conversely, with a high cost parameter value, two similar spike trains will be measured as having a large distance, i.e., they are considered dissimilar by the metric, due to the high cost of shifting spikes. While the measure presented in our work measures the response-relevant synchrony of the input spike trains of a neuron and by extension, the operational mode of that neuron, the spike train distance metrics measure the distance, or similarity between a pair or group of spike trains directly. However, both types of metrics can be used in different circumstances to measure the temporal precision of the neural code.

While similar work exists on measuring spike train correlations and synchrony, either by directly observing the spikes fired from a population of neurons (Grün, 2009; Staude, Rotter & Grün, 2010), or by identifying synchronous activity in local field po-

entials (Denker et al., 2011), our proposed measure differs in that it only responds to such correlations between spike trains converging into a single neuron, when they are responsible for the triggering of response spikes. In particular, our measure explicitly calculates the degree of input synchrony directly preceding a response spike and implicitly considers any previous activity by taking into account the potential at the start of the coincidence window  $w$  in the calculation. The higher the potential of the neuron’s membrane at the start of the coincidence window is, the lower the relative contribution of the synchronous spike trains within the coincidence window would be to the response. Consequently, the slope of the membrane potential within the coincidence window is low, denoting a higher contribution of temporal integration. In this way, our measure is only concerned with the input statistics that affect the neuron’s own spiking, in other words, it is sensitive to the response-relevant statistics of the input. It is this particular feature which links our measure’s estimation of response-relevant input synchrony to the underlying operational mode. The operational mode of a neuron is not defined solely by the synchrony of the spike trains it receives, but also by whether or not that synchronous activity causes firing.

Our study focused solely on excitatory inputs which caused the neuron to fire a response, in order to infer the degree of response-relevant synchrony specifically. This simplifying choice was made to establish the viability of the slope of the membrane potential in inferring pre-synaptic synchrony. The potential inclusion of inhibitory inputs in our models would require our methods, namely the slope bound calculations, to account for the effects of inhibition on the range of potentials the membrane can acquire. More specifically, inhibition can drive the membrane potential below  $V_{rest}$ , which can cause pre-spike membrane potential slopes with higher values than the ones the upper bound we have defined for this study (see eqns. (7) & (8)) could capture.

It should be noted that the intent of the work presented here is not to measure absolute input synchrony in itself. The value of  $\overline{M}$  is considerably less than 1 in cases where there is very high input synchrony ( $S_{in} \approx 1, \sigma_{in} \approx 0$ ), but the depolarisation caused by a single synchronous volley is not enough to cause a response. This occurs when the total number of input spike trains, combined with the level of depolarisation per spike, is insufficient to reach the firing threshold from rest, i.e.,  $N_{in}\Delta V_s < (V_{th} - V_{rest})$  (i.e., volleys are sub-threshold). In such a case, a series of two or more synchronous volleys

of spikes is required to cross the threshold, depending on the delay between each volley. The measure we have presented is therefore a measure of the synchrony between all input spikes that were responsible for any given response spike.

Generally, a neuron can operate in a sub- or super-threshold input regime. The different input regimes are defined in terms of the asymptotic time-averaged membrane potential  $\langle V \rangle$  in the absence of a threshold. If  $\langle V \rangle < V_{th}$ , the neuron is operating in a sub-threshold regime and spikes are caused by fluctuations which can briefly drive the membrane potential above threshold. Conversely, if  $\langle V \rangle > V_{th}$ , the neuron is operating in a super-threshold regime and spikes are fired quite regularly and inevitably by the integration of inputs (Gerstner & Kistler, 2002).

The mean membrane potential, again in the absence of a threshold, for our neuron is equal to  $\langle V \rangle = \Delta V_s N_{in} f_{in} \tau_m$ . However, we can also define the total contribution of a volley as  $\Delta V_v = N_{in} \Delta V_s$ . In our case however, by using synchronous volleys of input spikes, we can define four conditions, in terms of the aforementioned sub- and super-threshold regimes:

1. Case where  $\Delta V_v < V_{th}$  and  $\langle V \rangle < V_{th}$ .

This is analogous to a true sub-threshold regime where spikes are fired only in cases where two or more volleys arrive close enough for their combined contribution to reach the threshold. In other words, output spikes are caused by fluctuations in the arrival times of sub-threshold volleys. When these relations hold, our measure will not produce a value of  $M = 1$  when  $S_{in} = 1$  due to the contribution of each individual volley being sub-threshold. Spikes in such cases are caused with very low probability and depend on the timing of individual volleys and spikes, i.e., the fluctuations in the input. Fig. 3a corresponds to this case.

2. Case where  $\Delta V_v > V_{th}$  and  $\langle V \rangle < V_{th}$ .

If this is the case, then our measure will be able to achieve a value of 1 (if  $S_{in} = 1$ ), regardless of whether  $\langle V \rangle > V_{th}$  or not. Although this may correspond to a sub-threshold regime, the presence of super-threshold volleys makes firing of spikes a certainty and we can therefore refer to it as a *super-threshold volley regime*. Figs. 3c and 3e correspond to this case.

3. Case where  $\Delta V_v < V_{th}$  and  $\langle V \rangle > V_{th}$ .

In this interesting case, spikes are fired *almost surely* due to the neuron being in a

super-threshold regime, in the general sense, but our measure will never achieve  $\overline{M} = 1$ , due to the contribution of each individual volley being sub-threshold. Therefore, although the neuron is operating in a super-threshold regime, in terms of the contribution of single volleys it is operating in a *sub-threshold volley regime*. While the spikes within a single volley may coincide (highly synchronous volley, i.e.,  $S_{in} \approx 1$ ), the total dispersion between all the spikes that caused the neuron to fire is high. The value of  $\overline{M}$  reflects the total dispersion between all the contributing spikes, not the dispersion between spikes within a single volley. This emphasises the difference between input synchrony in the traditional sense and the response-relevant input synchrony, which we measure. The operational mode of a neuron is determined by the temporal dispersion of all the spikes that were responsible for the neuron's firing (Kisley & Gerstein, 1999; Rudolph & Destexhe, 2003). Fig. 3b corresponds to this case.

4. Case where  $\Delta V_v > V_{th}$  and  $\langle V \rangle > V_{th}$ .

In this case, the mean drive is very high as well as the depolarisation caused by individual volleys. The behaviour of the measure is the same as for case (2), as the mean drive has little effect on our measure as long as  $\Delta V_v$  is high enough to consistently cause a response. The measure however will behave unpredictably when the mean drive is strong enough to cause very high firing rates, as has been already discussed. Figs. 3d and 3f correspond to this case.

In summary, the correlation between input synchrony and  $\overline{M}$  is more dependent on the relationship between  $\Delta V_v$  and  $V_{th}$ , and is only slightly affected by the mean drive  $\langle V \rangle$ . When volleys have a total contribution which is sub-threshold (cases 1 and 2) then  $\overline{M} < 1$  even when  $S_{in} = 1$  and  $\sigma_{in} = 0$  ms. This reflects the fact that the response was caused by a number of volleys, each of which consisted of completely synchronised spikes, but whose total, summed inter-synchrony is much lower.

Our measure could be applied to membrane potential data generated by other, more complex, neuron models and it would be particularly interesting, after further refinement, to use this measure to provide insight into the operational mode and by extension, coding mechanisms employed by a real cortical neuron, using knowledge of the neuron's physiology and intracellular membrane potential data alone. Additionally it would be interesting to study the measure itself further and how it can be extended to provide more information on the inner workings of a neuron. It would most likely

be more informative and it could help make stronger inferences concerning the input statistics, if the distribution of  $M$  values is studied instead of the average value alone.

## Appendix A

### *Upper and lower bound convergence at high firing rates*

In this Appendix we demonstrate that the indicative membrane potential slopes ( $U_i$  and  $L_i$ ) associated with the two operational modes, temporal integration and coincidence detection, converge onto each other at high firing rates. The level of convergence is dependent on the length of the coincidence window ( $w$ ), which reflects the assumed temporal precision of the neural code. From this convergence it follows that, at very high firing rates, the two operational modes become indistinguishable. The purpose of this Appendix is to formally describe this convergent behaviour.

In order to grasp the intuition behind this phenomenon, let us first consider the case where a firing ISI is equal to the coincidence window, i.e.,  $\Delta t_i = w$ . In this case, it is clear from eqns. (6) and (8) that  $U_i = L_i$ , i.e., the two operational modes are described by the exact same slope value and are therefore identical and indistinguishable.

More generally, at very high firing rates the ISIs are much shorter than the membrane leak time constant ( $\Delta t_i \ll \tau_m$ ). When this holds, the solution of eqn. (1) for constant input given below

$$V(t) = V_{rest} + IR \left( 1 - \exp \left( -\frac{t - t_0}{\tau_m} \right) \right), \quad (10)$$

can have its leak term replaced by an approximation of the term's Taylor series expansion as shown in eqn. (11).

$$\exp \left( -\frac{t - t_0}{\tau_m} \right) \approx 1 - \frac{t - t_0}{\tau_m} \quad (11)$$

Therefore, from eqns. (10) and (11), the membrane potential equation of the LIF model is simplified and approximated by eqn. (12).

$$V'(t) = V_{rest} + \frac{I(t - t_0)}{C} \quad (12)$$

where the prime here signifies the membrane potential of the approximating model and  $C$  is the capacitance of the membrane.

This approximating model is the perfect (i.e., non-leaky) Integrate-and-Fire neuron model (PIF), which simply integrates post-synaptic inputs, without losing any of its charge over time. We then use the two equations (10) & (12) to calculate the relative difference between the two models as a function of the ISI ( $\Delta t_i$ ). The relative difference is measured at the beginning of the pre-spike coincidence window, because the membrane potential at this time determines the slope of the secant line associated with that specific spike (see eqn. (3) and fig. 2a). Therefore, the relative difference for any given ISI is calculated as the difference between the two models at the beginning of the coincidence window, i.e.,  $t_i - w$  (eqn. (13)).

$$d_{t_i, w} = \frac{|V(t_i - w) - V'(t_i - w)|}{V(t_i - w)} \quad (13)$$

where  $V(t)$  and  $V'(t)$  are given by eqns. (10) and (12) respectively. The relative difference is used as a measure of dissimilarity between the two models and by extension, it measures the distinguishability between the two operational modes. The higher the relative difference, the more distinguishable the two operational modes are and vice versa. Therefore, the relative difference  $d$  represents the level of divergence between the LIF and PIF.

Fig. 5 shows the relative difference  $d$  (eqn. (13)), as a function of the ISI ( $\Delta t_i$ ) at high firing rates, for a coincidence window length  $w = 2$  ms. Note that changing the length of the coincidence window  $w$  shifts  $d$  along the horizontal axis, i.e., increasing the window length moves the curve to the right and decreasing the window length moves the curve to the left. By decreasing the coincidence window length, we could effectively increase the relative difference for the same values of  $\Delta t_i$ , thus improving the distinguishability of operational modes at higher rates. A coincidence window of the order of microseconds, indicating a very high temporal precision of firing, is experimentally observed and used in models of coincidence detectors in the auditory system (Gerstner et al., 1996; Oertel et al., 2000; Marsalek & Lánský, 2005). However, for neurons with membrane time constants between 10–20 ms (as in our study, where  $\tau_m = 10$  ms), the temporal precision is considered to be between 1–3 ms (Gerstner et al., 1996).

## Appendix B

*Analysis of the behaviour of the LIF neuron with partial reset at high firing rates.*

In this Appendix we demonstrate how the partial reset mechanism of the LIFwPR model effectively reduces the number of input spikes  $N'_{th}$  required to cause a LIF neuron to fire and results in a very short effective membrane time constant  $\tau'_m$ . These effects are relevant whenever the membrane potential of the neuron  $V(t)$  is above the partial reset potential  $V_{reset}$ . While this may not hold true for the entirety of a simulation, for the high firing rate regime explored using this model, the membrane potential remains above the reset value for most of the time and for extended continuous periods of increased activity.

We use the definition of  $N_{th}$  in the same way as Softky & Koch (1993), who described their models in terms of the difference in potential between threshold and rest, divided by the depolarisation per spike, as in eqn. (14):

$$N_{th} = \frac{V_{th} - V_{rest}}{\Delta V_s} \quad (14)$$

This is done in order to make our results comparable with their analysis, which showed how the coefficient of variation (CV) varied as a function of the time constant  $\tau_m$  and  $N_{th}$  (see fig. 8 in Softky & Koch, 1993).

Assuming that  $V_{reset} \geq V_{rest}$  (which holds for any model with a reset parameter  $\beta \geq 0$ ), for any given time where  $V(t) \geq V_{reset}$ , the model neuron can be expressed in terms of an equivalent model with effective resting potential  $V'_{rest} = V_{reset}$  and effective time constant  $\tau'_m$  (the prime signifies a parameter or variable of the equivalent model). From this, it follows that  $N'_{th} \leq N_{th}$ , since  $V'_{rest} \geq V_{rest}$  as it can be seen from eqn. (15)

$$N'_{th} = \frac{V_{th} - V'_{rest}}{\Delta V_s} = N_{th}(1 - \beta) \quad (15)$$

Substituting for the parameter values used for our simulations, i.e.,  $V_{th} = 15$  mV,  $V_{rest} = 0$  mV and  $\Delta V_s = 0.16$  mV, the original value of  $N_{th}$  is approximately 94. For  $V'_{rest} = 13.65$  mV however, which is the reset value of the LIFwPR model where  $\beta = 0.91$ , the effective number of input spikes required to fire a spike  $N'_{th}$  is reduced to just 9 (approximately).

The effective time constant's value  $\tau'_m$  should be such that (assuming the inputs are the same for both models) the change in membrane potential within a fixed period of

time in the equivalent model should be equal to that of the original model,  $\frac{dV}{dt} = \frac{dV'}{dt}$ . Since the two models share the same input, we can calculate  $\tau'_m$  by ignoring the input terms of the two models and equating the leak term of eqn. (1) with the leak term of the equivalent model (eqn. (16)):

$$\frac{dV'}{dt} = -\frac{V(t) - V'_{rest}}{\tau'_m} \quad (16)$$

Equating eqns. (1) and (16), replacing the effective resting value  $V'_{rest}$  with the original reset value  $V_{reset}$  and solving for  $\tau'_m$  gives eqn. (17):

$$\tau'_m = \tau_m \frac{V(t) - V_{reset}}{V(t) - V_{rest}} \quad (17)$$

Therefore the value of the effective time constant  $\tau'_m$  constantly changes as a function of the membrane potential  $V(t)$ . For our simulations, we can calculate the range of values that  $\tau'_m$  takes, first by substituting the parameter values we used, i.e.,  $\tau_m = 10$  ms,  $V_{rest} = 0$  mV and  $V_{reset} = 13.65$  mV and then by calculating  $\tau'_m$  for the known range of  $V(t)$  using eqn. (17). Thus, for our simulations  $\tau'_m = 10(V(t) - 13.65)/V(t)$ .

Since the effects discussed here are relevant for membrane potential levels above the reset potential, for our simulations we calculate the range of  $\tau'_m$  for membrane potential values between  $V(t) \in [V_{reset}, V_{th}] = [13.65 \text{ mV}, 15 \text{ mV}]$  giving respective  $\tau'_m \in [0 \text{ ms}, 0.9 \text{ ms}]$ .

## Acknowledgments

We gratefully acknowledge the support of the University of Cyprus for an Internal Research Project Grant. We are also grateful to the two anonymous referees for their constructive and stimulating reviews.

## References

- Abeles, M. (1982). Role of the cortical neuron: integrator or coincidence detector? *Israel Journal of Medical Sciences*, 18, 83–92.

- Aertsen, A., Diesmann, M. & Gewaltig, M. O. (1996). Propagation of synchronous spiking activity in feedforward neural networks. *Journal of Physiology-Paris*, 90(3-4), 243–247.
- Berger, D., Borgelt, C., Louis, S., Morrison, A., & Grün, S. (2010). Efficient Identification of Assembly Neurons within Massively Parallel Spike Trains. *Computational Intelligence and Neuroscience*, 439648.
- Bugmann, G., Christodoulou, C. & Taylor, J. G. (1997). Role of temporal integration and fluctuation detection in the highly irregular firing of a leaky integrator neuron model with partial reset. *Neural Computation*, 9, 985–1000.
- Buzsáki, G., & Draguhn, A. (2004). Neuronal oscillations in cortical networks. *Science*, 304(5679), 1926–1929.
- Christodoulou, C., Clarkson, T. G., Bugmann, G. & Taylor, J. G. (2000). Analysis of fluctuation-induced firing in the presence of inhibition. In Proceedings of the International Joint Conference on Neural Networks 2000 Vol.III, pp. 115–120. San Mateo, CA: IEEE Computer Society Press.
- Christodoulou, C. & Bugmann, G. (2001). Coefficient of variation (CV) vs mean interspike interval (ISI) curves: what do they tell us about the brain? *Neurocomputing*, 38–40, 1141–1149.
- Christodoulou, C. & Cleanthous, A. (2011). Does high firing irregularity enhance learning? *Neural Computation*, 23(3), 656–663.
- Cleanthous, A. & Christodoulou, C. (2012). Learning optimisation by high firing irregularity. *Brain Research*, 1434, 115–122.
- Crick, F., & Koch, C. (1990). Towards a neurobiological theory of consciousness. *Seminars in the Neurosciences*, 2, 263–275.
- Denker, M., Roux, S., Lindén, H., Diesmann, M., Riehle, A. & Grün, S. (2011). The local field potential reflects surplus spike synchrony. *Cerebral Cortex*, 21, 2681–2695.

- DeWeese, M. R. & Zador, A. M. (2006). Non-gaussian membrane potential dynamics imply sparse, synchronous activity in auditory cortex. *Journal of Neuroscience*, *26*(47), 12206–12218.
- Faes, C., Geys, H., Molenberghs, G., Aerts, M., Cadarso-Suárez, C., Acuña, C., & Cano, M. (2008). A flexible method to measure synchrony in neuronal firing. *Journal of the American Statistical Association*, *103*(481), 149–161.
- Gerstner, W., & Kistler, W. M. (2002). *Spiking Neuron Models*. Cambridge University Press, Cambridge.
- Gerstner, W., Kempter, R., van Hemmen, J. L. & Wagner, H. (1996). A neuronal learning rule for sub-millisecond temporal coding. *Nature*, *383*, 76–78.
- Goedeke, S., & Diesmann, M. (2008). The mechanism of synchronization in feed-forward neuronal networks. *New Journal of Physics*, *10*, 015007.
- Grün, S. (2009). Data-driven significance estimation for precise spike correlation. *Journal of Neurophysiology*, *101*, 1126–1140.
- Grün, S., Diesmann, M., & Aertsen, A. (2010). Unitary Event Analysis. In S. Grün & S. Rotter (Eds.), *Analysis of Parallel Spike Trains* (pp. 191–220). New York, NY: Springer.
- Kanev, J., Wenning, G., & Obermayer, K. (2004). Approximating the response-stimulus correlation for the integrate-and-fire neuron. *Neurocomputing*, *58-60*, 47-52.
- Kisley, M. A. & Gerstein, G. L. (1999). The continuum of operating modes for a passive model neuron. *Neural Computation*, *11*, 1139–1154.
- Kobayashi, R., Shinomoto, S., & Lánský, P. (2011). Estimation of time-dependent input from neuronal membrane potential. *Neural Computation*, *23*(12), 3070–3093.
- König, P., Engel, A. K. & Singer, W. (1996). Integrator or coincidence detector? The role of the cortical neuron revisited. *Trends in Neurosciences*, *19*, 130–137.

- Kostal, L., Lánský, P., & Rospars, J. P. (2007). Neuronal coding and spiking randomness. *European Journal of Neuroscience*, *26*(10), 2693–2701.
- Kreuz, T., Chicharro, D., Greschner, M., & Andrzejak, R. G. (2011). Time-resolved and time-scale adaptive measures of spike train synchrony. *Journal of Neuroscience Methods*, *195*, 92–106.
- Kuhn, A., Rotter, S., & Aertsen, A. (2002). Correlated input spike trains and their effects on the response of the leaky integrate-and-fire neuron. *Neurocomputing*, *44*, 121–126.
- Lánský, P. & Smith, C. E., (1989). The effect of a random initial value in neural first-passage-time models. *Mathematical Biosciences*, *23*(2), 191–215.
- Lánský, P. & Musila, M. (1991). Variable initial depolarization in Stein's neuronal model with synaptic reversal potentials. *Biological Cybernetics*, *64*, 285–291.
- Lánský, P. & Rodriguez, R. (1999). Two-compartment stochastic model of a neuron. *Physica D*, *132*, 267–286.
- Lapicque, L. (1907). Recherches quantitatives sur l'excitation électrique des nerfs traitée comme une polarisation. *Journal de Physiologie et de Pathologie Generale*, *9*, 620–635.
- Mainen, Z. F. & Sejnowski, T. J. (1995). Reliability of spike timing in neocortical neurons. *Science*, *268*, 1503–1506.
- Marsalek, P. & Lánský, P. (2005). Proposed mechanisms for coincidence detection in the auditory brainstem. *Biological Cybernetics*, *92*, 445–451.
- Mitchell, C. C. (2005). Precision of neural timing: The small  $\epsilon$  limit. *Journal of Mathematical Analysis and Applications*, *309*, 567–582.
- Oertel, D., Bal, R., Gardner, S. M., Smith, P. H. & Joris, P. X. (2000). Detection of synchrony in the activity of auditory nerve fibers by octopus cells of the mammalian cochlear nucleus. *Proceedings of the National Academy of Sciences*, *97*(22), 11773–11779.

- Perkel, D. H., Gerstein, G. L., & Moore, G. P. (1967a). Neuronal spike trains and stochastic point processes I. The single spike train. *Biophysical Journal*, 7(4), 391–418.
- Perkel, D. H., Gerstein, G. L., & Moore, G. P. (1967b). Neuronal spike trains and stochastic point processes II. Simultaneous spike trains. *Biophysical Journal*, 7(4), 419–440.
- Reed, M. C., Blum, J. J. & Mitchell, C. C. (2002). Precision of neural timing: Effects of convergence and time-windowing. *Journal of Computational Neuroscience*, 13, 35–47.
- Rospars, J. P. & Lánský, P. (1993). Stochastic neuron model without resetting of dendritic potential: Application to the olfactory system. *Biological Cybernetics*, 69, 283–294.
- Rotter, S., & Diesmann, M. (1999). Exact digital simulation of time-invariant linear systems with applications to neuronal modeling. *Biological Cybernetics*, 81(5-6), 381–402.
- Rudolph, M. & Destexhe, A. (2003). Tuning neocortical pyramidal neurons between integrators and coincidence detectors. *Journal of Computational Neuroscience*, 14(3), 239–251.
- Salinas, E., & Sejnowski, T. J. (2001). Correlated neuronal activity and the flow of neural information. *Nature Reviews Neuroscience*, 2(8), 539–550.
- Salinas, E., & Sejnowski, T. J. (2002). Integrate-and-fire neurons driven by correlated stochastic input. *Neural Computation*, 14(9), 2111–2155.
- Schrader, S., Grün, S., Diesmann, M., & Gerstein, G. L. (2008). Detecting synfire chain activity using massively parallel spike train recording. *Journal of Neurophysiology*, 100(4), 2165–2176.

- Shadlen, M. & Newsome, W. (1994). Noise, neural codes and cortical organization. *Current Opinion on Neurobiology*, 4(4), 569–579.
- Shadlen, M. N., & Newsome, W. T. (1995). Is there a signal in the noise? *Current Opinion in Neurobiology*, 5, 248–250.
- Shadlen, M. & Newsome, W. (1998). The variable discharge of cortical neurons: implications for connectivity, computation, and information coding. *Journal of Neuroscience*, 18(10), 3870–3896.
- Singer, W. (1999). Neuronal synchrony: A versatile code for the definition of relations? *Neuron*, 24(1), 49–65.
- Softky, W. & Koch, C. (1992). Cortical cells should fire regularly, but do not. *Neural Computation*, 4, 643–646.
- Softky, W. & Koch, C. (1993). The highly irregular firing of cortical cells is inconsistent with temporal integration of random EPSPs. *Journal of Neuroscience*, 13(1), 334–350.
- Stark, E., & Abeles, M. (2009). Unbiased estimation of precise temporal correlations between spike trains. *Journal of Neuroscience Methods*, 179(1), 90–100.
- Stauder, B., Rotter, S. & Grün, S. (2010). CUBIC: Cumulant based inference of higher-order correlations in massively parallel spike trains. *Journal of Computational Neuroscience*, 29(1–2), 327–350.
- Stein, R. B. (1965). A theoretical analysis of neuronal variability. *Biophysical Journal*, 5(2), 173–194.
- Stein, R. B. (1967). Some models of neuronal variability. *Biophysical Journal*, 7, 37–68.
- Stein, R. B., Gossen, E. R., & Jones, K. E. (2005). Neuronal variability: noise or part of the signal? *Nature Reviews Neuroscience*, 6(5), 389–397.

- Tuckwell, H. C. (1988). *Introduction to Theoretical Neurobiology: Volume 1, Linear Cable Theory and Dendritic Structure*. Cambridge University Press, Cambridge.
- Usrey, W. M., & Reid, R. C. (1999). Synchronous activity in the visual system. *Annual Review of Physiology*, 61(1), 435–456.
- Victor, J. D. & Purpura, K. P. (1996). Nature and precision of temporal coding in visual cortex: A metric-space analysis. *Journal of Neurophysiology*, 76(2), 1310–1326.
- Victor, J. D. (2005). Spike train metrics. *Current Opinion in Neurobiology*, 15, 585–592.
- von der Malsburg, C. (1981). The correlation theory of brain function. Internal Report 81-2, Department of Neurobiology, Max Planck Institute for Biophysical Chemistry, Göttingen, Federal Republic of Germany.
- Wilbur, A. J. & Rinzel, J. (1983). A theoretical basis for large coefficient of variation and bimodality in neuronal interspike interval distribution. *Journal of Theoretical Biology*, 105, 345–368.
- Wilson, H. R. (1999). *Spikes, decisions & actions: Dynamical foundations of neuroscience*. New York, NY: Oxford University Press.

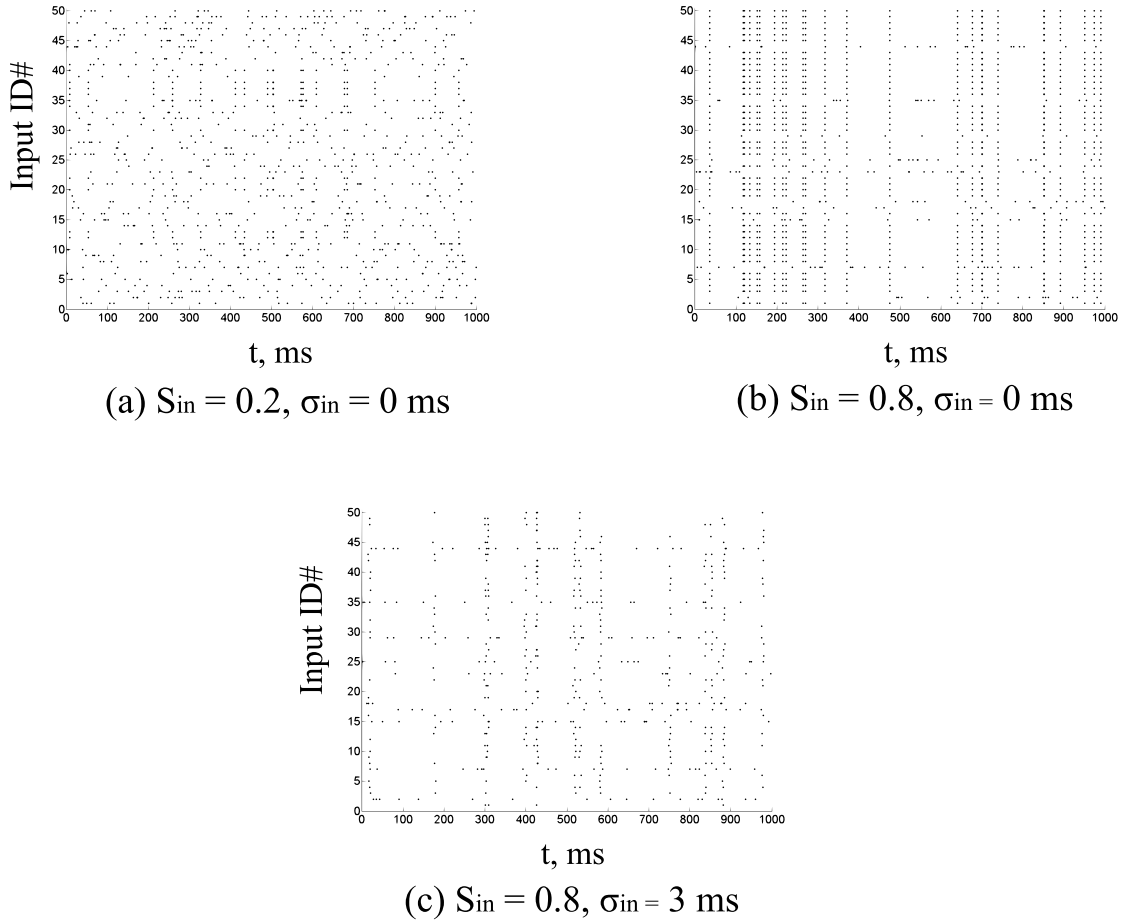


Figure 1: Three sample input cases showing the effects of the two synchrony parameters  $S_{in}$  &  $\sigma_{in}$  (see text for details) on the overall temporal structure of the input spike trains. For all three cases,  $N_{in} = 50$  and  $T = 1000$  ms. The first raster plot (a) shows a mostly random set of spike trains, with only 20 % of the spike trains being completely synchronised ( $S_{in} = 0.2$ ). The second plot (b) shows a much higher degree of synchrony with 80 % of the spike trains being identical ( $S_{in} = 0.8$ ). The third plot (c) shows the effects of high jitter ( $\sigma_{in} = 3$  ms) on spike trains with 80 % synchrony ( $S_{in} = 0.8$ ). Comparing (c) to (b), while it is apparent by the vertical columns of aligned spikes that there is a high amount of synchrony in both, the existence of Gaussian jitter in (c) makes the overall spike trains more noisy and the columns are less pronounced.

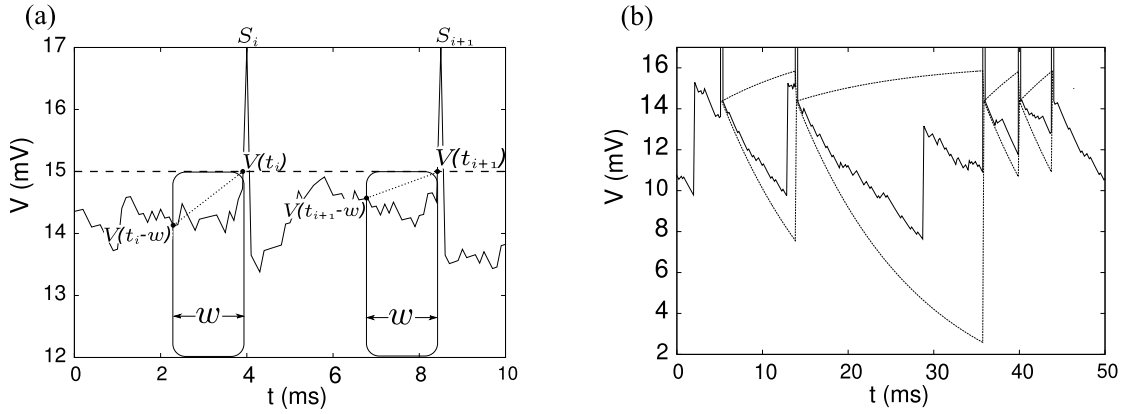


Figure 2: Two example membrane potential traces  $V(t)$  for the LIFwPR model.

(a) Pre-spike windows ( $w$ ) and related secant lines (dotted lines) are shown. The first secant line which corresponds to the first spike ( $S_i$ ) starts at  $V(t_i - w)$  and ends at  $V(t_i)$ . The second secant line which corresponds to the second spike ( $S_{i+1}$ ) starts at  $V(t_{i+1} - w)$  and ends at  $V(t_{i+1})$ . The dashed horizontal line denotes the membrane potential firing threshold  $V_{th}$  (15 mV).

(b) The two bounds are shown between each pair of consecutive spikes. The lower bound (low slope) corresponds to a dotted line starting at the post-spike reset potential (in this case,  $V_{reset} = 13.65$  mV) and ending at the point where the potential crossed the threshold ( $V_{th} = 15$  mV). The upper bound (high slope) corresponds to a dotted curve which decays from the post-spike reset potential for the duration of the ISI. The two bounds correspond to the theoretical trajectory of the membrane in the presence of constant input for the lower bound and completely synchronised inputs, with no background activity, for the upper bound.

In principle, input spikes cause instantaneous jumps and  $V(t)$  should appear discontinuous on the plots. However, since  $V(t)$  was simulated numerically, instantaneous jumps become one time-step wide and are plotted as continuous lines for simplicity, on both sub-figures.

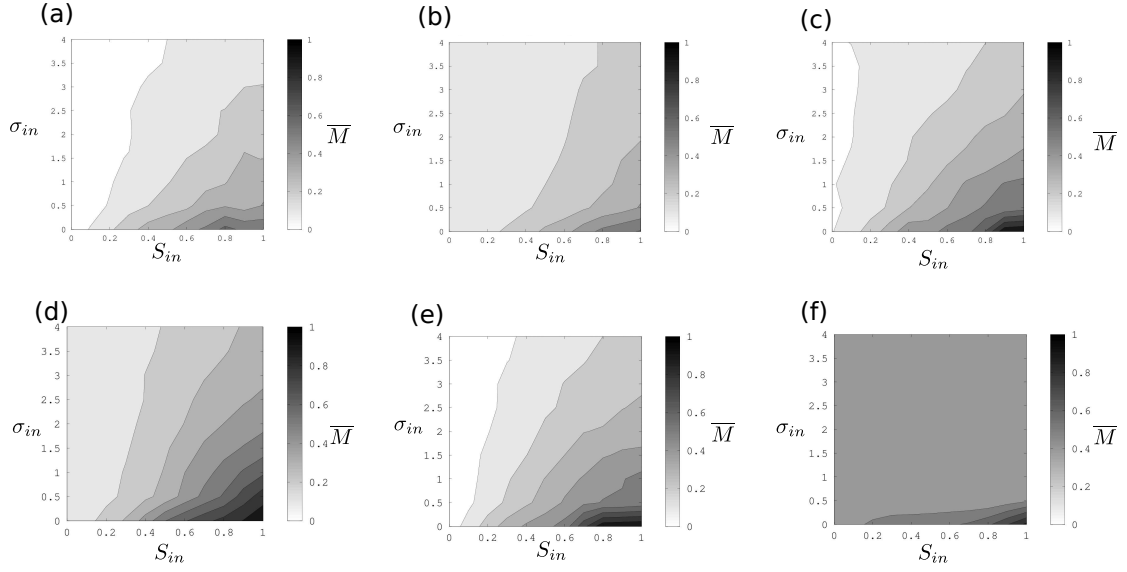


Figure 3: The normalised pre-spike membrane potential slope ( $\overline{M}$ ) for a LIF neuron model with total reset. For each plot, the firing rate of the LIF neuron is kept constant by calibrating the rate of the input spike trains at each data point. All the input spike trains were calibrated simultaneously and always shared the same mean rate. The parameters for the plots were as follows: (a)  $N_{in} = 100$ ,  $\Delta V_s = 0.1$  mV,  $f_{out} = 5$  Hz ( $f_{in} = 16$ – $138$  Hz), (b)  $N_{in} = 50$ ,  $\Delta V_s = 0.2$  mV,  $f_{out} = 100$  Hz ( $f_{in} = 218$ – $465$  Hz), (c)  $N_{in} = 60$ ,  $\Delta V_s = 0.3$  mV,  $f_{out} = 10$  Hz ( $f_{in} = 10$ – $78$  Hz), (d)  $N_{in} = 60$ ,  $\Delta V_s = 0.5$  mV,  $f_{out} = 70$  Hz ( $f_{in} = 65$ – $113$  Hz), (e)  $N_{in} = 200$ ,  $\Delta V_s = 0.1$  mV,  $f_{out} = 10$  Hz ( $f_{in} = 10$ – $74$  Hz), (f)  $N_{in} = 60$ ,  $\Delta V_s = 0.5$  mV,  $f_{out} = 400$  Hz ( $f_{in} = 250$ – $755$  Hz). The horizontal axis shows the proportion of synchronised spike trains ( $S_{in} \in [0, 1]$ ), while the vertical axis shows the amount of jitter applied to the synchronous spikes ( $\sigma_{in} \in [0, 4]$  ms). The grey-scale indicates the value of  $\overline{M}$  for the simulation, with lighter regions having lower values denoting temporal integration and darker regions having higher values denoting coincidence detection, as shown by the grey-scale bar on the right side of each plot.

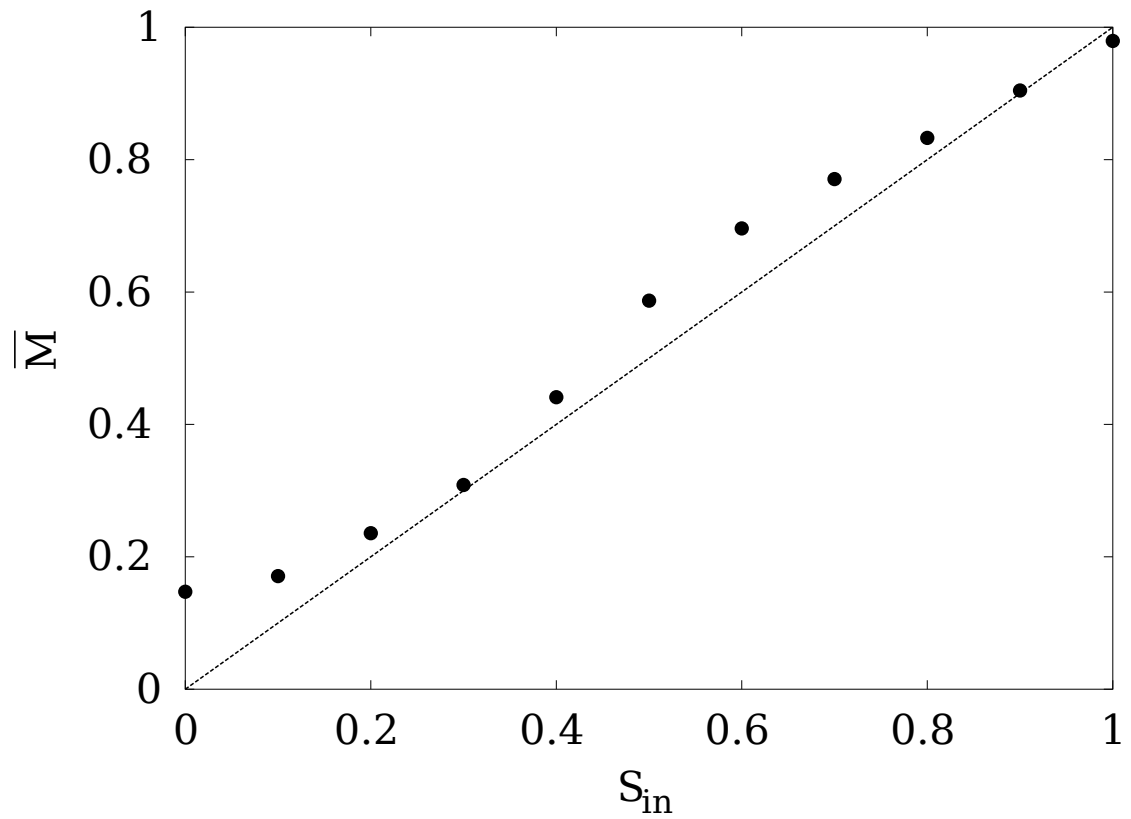


Figure 4: Normalised pre-spike membrane potential slope ( $\bar{M}$ ) for  $\sigma_{in} = 0$ , plotted against the full range of  $S_{in}$  values. The circles represent measured data points for the LIF neuron firing at 70 Hz (corresponding to fig. 3d), while the line represents perfect linear correlation for comparison.

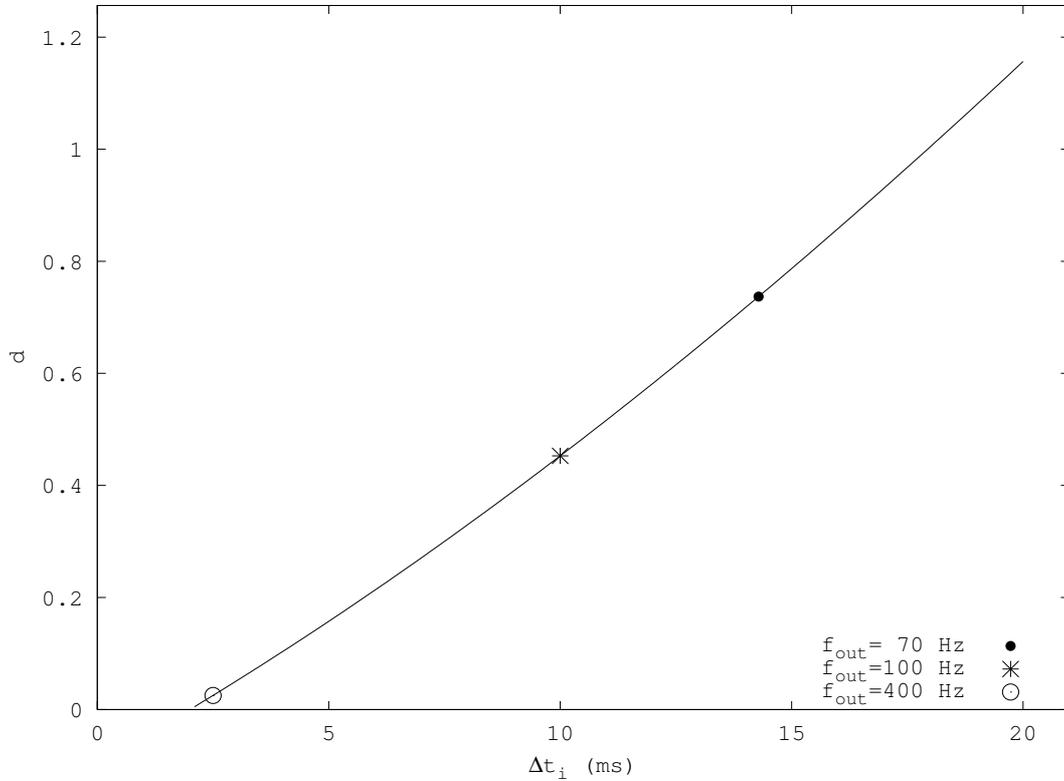


Figure 5: Relative difference ( $d$ ) between the LIF and the perfect integrator models as a function of firing ISI ( $\Delta t_i$ ), for window length  $w = 2$  ms (solid line). For details on the derivation of the relative difference ( $d$ ) see Appendix A and more specifically eqn. (13). The three points marked in the graph correspond to the firing rates of the simulations which produced figs. 3b, (100 Hz), 3d (70 Hz) and 3f (400 Hz). As we are interested in the relative difference at high firing rates, the graph does not show the points corresponding to the firing rates of the simulations which produced figs. 3a (i.e., 5 Hz corresponding to  $\Delta t_i$  of 200 ms) and 3c and 3e (i.e., 10 Hz corresponding to  $\Delta t_i$  of 100 ms). Note that changing the length of the coincidence window  $w$  shifts the relative difference  $d$  along the horizontal axis, i.e., increasing the window length moves the curve to to the right and decreasing the window length moves the curve to the left.

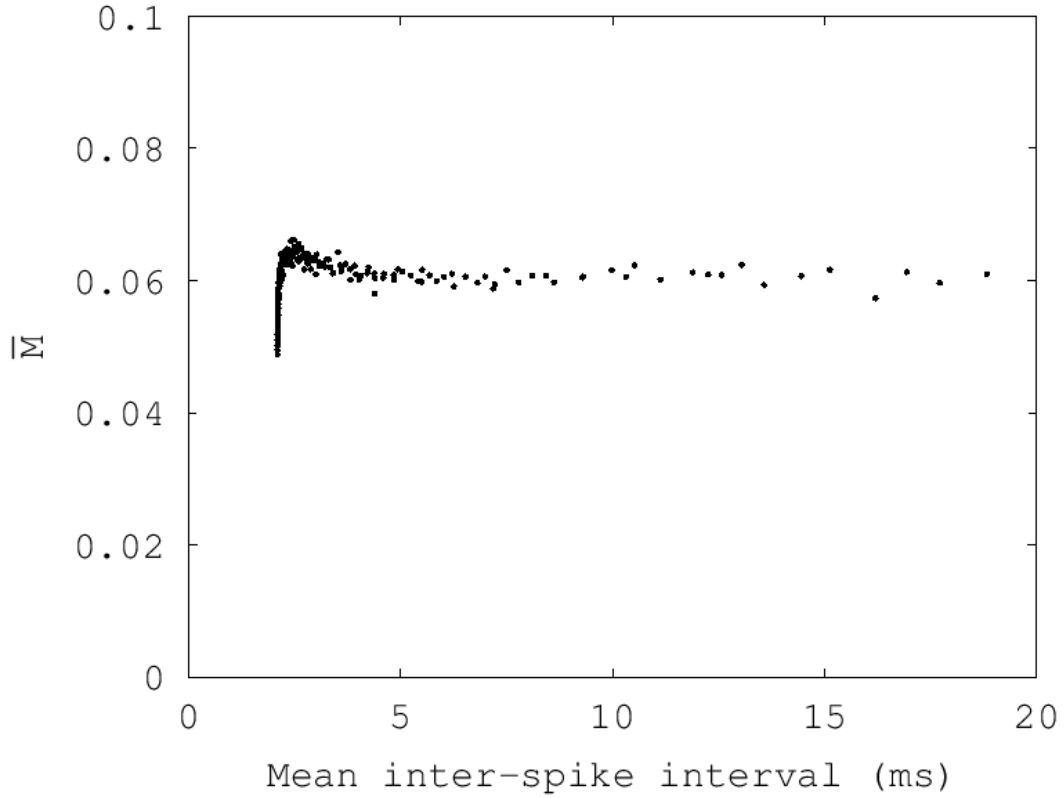


Figure 6: The normalised pre-spike membrane potential slope ( $\bar{M}$ ) for the LIFwPR model firing highly irregularly at rates up to  $\sim 470$  Hz (mean ISI  $\approx 2.1$  ms). Each point on the plot shows the value of  $\bar{M}$  (vertical axis) for the LIFwPR with parameters as described in the text (see Table 1) for a given firing ISI ( $1/f_{out}$ ). The firing rates were achieved by varying the input rates  $f_{in}$  within physiological ranges to achieve the various output firing rates,  $f_{out}$ . The results show that  $\bar{M}$  is always below 0.1 ( $\bar{M} \approx 0.06$  on average), for the entire range of firing rates. This suggests that the model neuron, when firing highly irregularly at high rates, operates mainly as a temporal integrator.